AIP | Applied Physics Letters

Magneto-ballistic transport in GaN nanowires

Giovanni Santoruvo, Adrien Allain, Dmitry Ovchinnikov, and Elison Matioli

Citation: Applied Physics Letters **109**, 103102 (2016); doi: 10.1063/1.4962332
View online: http://dx.doi.org/10.1063/1.4962332
View Table of Contents: http://scitation.aip.org/content/aip/journal/apl/109/10?ver=pdfcov
Published by the AIP Publishing

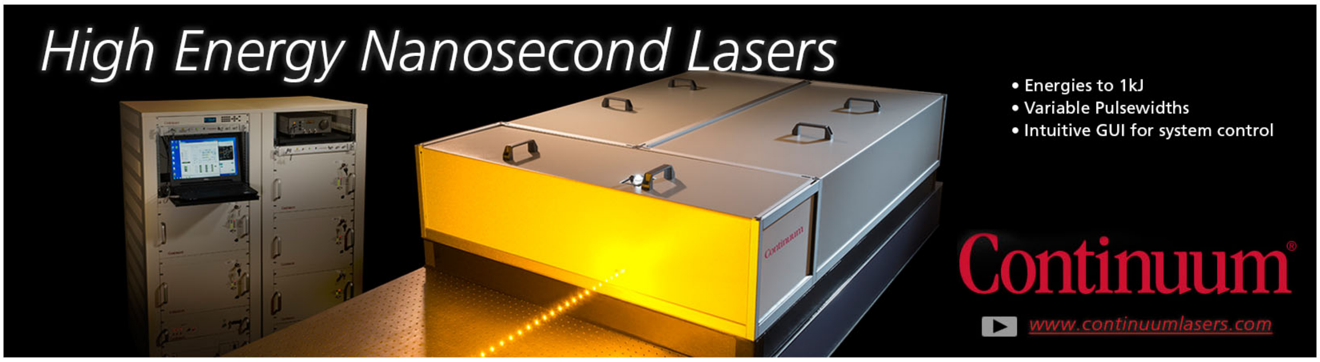

APPLIED PHYSICS LETTERS **109**, 103102 (2016)

Magneto-ballistic transport in GaN nanowires

Giovanni Santoruvo,[a)] Adrien Allain, Dmitry Ovchinnikov, and Elison Matioli[b)]
Ecole Polytechnique Fédérale de Lausanne (EPFL), CH 1015 Lausanne, Switzerland

(Received 12 July 2016; accepted 24 August 2016; published online 7 September 2016)

The ballistic filtering property of nanoscale crosses was used to investigate the effect of perpendicular magnetic fields on the ballistic transport of electrons on wide band-gap GaN heterostructures. The straight scattering-less trajectory of electrons was modified by a perpendicular magnetic field which produced a strong non-linear behavior in the measured output voltage of the ballistic filters and allowed the observation of semi-classical and quantum effects, such as quenching of the Hall resistance and manifestation of the last plateau, in excellent agreement with the theoretical predictions. A large measured phase coherence length of 190 nm allowed the observation of universal quantum fluctuations and weak localization of electrons due to quantum interference up to ∼25 K. This work also reveals the prospect of wide band-gap GaN semiconductors as a platform for basic transport and quantum studies, whose properties allow the investigation of ballistic transport and quantum phenomena at much larger voltages and temperatures than in other semiconductors. *Published by AIP Publishing.*
[http://dx.doi.org/10.1063/1.4962332]

Ballistic transport of electrons has attracted great interest for high frequency and low power electronic devices due to the possibility of electrons moving without any scattering from lattice defects, phonons, impurities, and other sources of scattering.[1] This regime occurs when electrons travel a distance shorter than their mean free path l_m (average distance between consecutive scattering events), which can be as small as tens of nanometers depending on the material. Therefore, ballistic transport is a nanoscale phenomenon, requiring nanoscale structures.

Ballistic transport has been exploited for new kinds of electronic devices such as ballistic rectifiers and artificial functional materials,[2] ballistic deflections transistors,[3] and logic gates using quantum point contacts.[4] Narrow-gap semiconductors presenting high electron mobility have been commonly used to investigate ballistic transport, such as InGaAs/InP,[2] GaAs/AlGaAs,[5] InSb/AlInSb,[6] InAs,[7] and Si/SiGe.[8] Cryogenic temperature measurements led to the discovery of several phenomena, such as the quantized conductance in a point contact,[9,10] electron focusing,[11] negative bend resistance,[12,13] quantum Hall effect,[14] and quantum interference.[15]

The large optical phonon energy (E_{OP}) combined with the high electron mobility observed in wide band-gap GaN semiconductors allow the investigation of ballistic transport at larger voltages and temperatures than in other semiconductors. In this work, the ballistic filtering property of nanoscale crosses demonstrated on AlGaN/GaN heterostructures[16] was used to investigate the effect of a strong perpendicular magnetic field on the straight scattering-less trajectories of ballistic electrons, motivated by the strong analogy of ballistic transport in semiconductors and electrons moving in vacuum tubes[17] whose trajectory can be easily deflected by electromagnetic lens. Under large bias conditions ($V_{bias} \gg E_f/q$, where E_f is the Fermi energy), the presence of a perpendicular magnetic field caused electrons to move ballistically in cyclotron orbits, whose radius could be modified by sweeping either the applied bias or the magnetic field. The deflection of the electron trajectories together with the shape of the device produced a strong non-linear behavior when the electron trajectories changed from straight to circular.

The absence of scattering is also a required condition for the manifestation of semi-classical and quantum phenomena. Hall measurements performed in the same device under small-bias conditions permitted the observation of a plateau in the Hall resistance under small magnetic fields, while at large magnetic fields edge states generated a second plateau, known as "last plateau" with reference to the Quantum Hall effect. Moreover, quantum fluctuations in both the longitudinal and transversal resistances were observed due to quantum interference phenomena.

The device was fabricated on an epitaxial structure composed of $Al_{0.25}Ga_{0.75}N$ (25 nm)/AlN (8 nm)/GaN on silicon substrate, where the two-dimensional electron gas (2DEG) is present below the AlGaN/GaN interface (right inset of Fig. 1). Nanoscale crosses with width of 87 nm were defined by

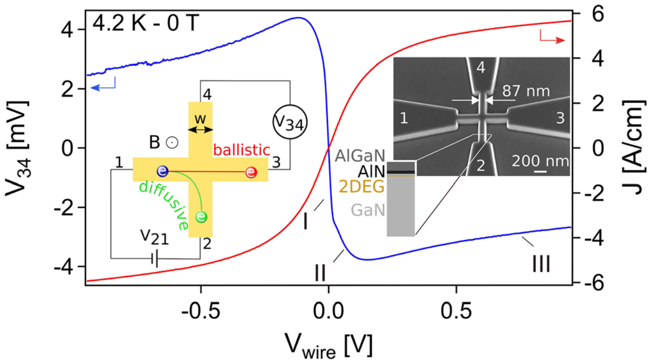

FIG. 1. V_{34} and J versus V_{wire} at 4.2 K and 0 T highlighting three regions: ballistic region characterized by the negative slope of V_{34} (I); transition region where optical phonon emission causes both the change of slope of V_{34} and the saturation of J (II); and diffusive region where drift transport dominates (III). In the left inset, the schematic shows the measurement set up and electron path under ballistic and diffusive transport with a 16°-tilted SEM picture of the device (right inset).

[a)]giovanni.santoruvo@epfl.ch
[b)]elison.matioli@epfl.ch

electron-beam lithography using hydrogen silsesquioxane 2% (HSQ), acting both as e-beam resist and hard mask for the subsequent etching process. Mesa and nanoscale crosses, with depth of 200 nm, were etched by inductively coupled plasma (ICP) using Cl_2. For the ohmic contacts, a metal stack of Ti (200 Å)/Al (1000 Å)/Ni (250 Å)/Au (500 Å) was deposited on the contact regions and annealed at 875 °C.

Electron mobility (μ_e), carrier concentration (n_s), and sheet resistance (R_{sh}) measured at 300 K (4.2 K) by square Hall patterns ($180\,\mu m \times 180\,\mu m$) were $6.62 \times 10^{12}\,cm^{-2}$ ($7.62 \times 10^{12}\,cm^{-2}$), 1748 $cm^2/V\,s$ (10 702 $cm^2/V\,s$), and 540.2 $\Omega/\square$ (76.5 $\Omega/\square$). The contact resistance (R_c) measured by transmission line measurements (TLM) was 0.26 Ωmm at 300 K and 0.37 Ωmm at 4.2 K. The parasitic resistance (R_p), defined as the sum of the contact and access resistances in the trapezoidal arms (right inset of Fig. 1), was calculated from R_c and R_{sh}, resulting in 11.29 kΩ at 300 K and 2.18 kΩ at 4.2 K. The voltage drop in the nanoscale crosses was determined after removing the voltage drop in R_p as $V_{wire} = V_{21} - R_p I_2$. From the carrier concentration and mobility, the Fermi wavevector and velocity (k_F, v_F) and the mean free path (used later in this work) were calculated using the following expressions: $k_F = \sqrt{2\pi n_s}$, $v_F = \hbar k_F/m^*$, $l_m = m^* \mu_e v_f/q$.

The nature of the electron transport in the nanoscale cross (right inset of Fig. 1(a)), which functions as a filter for ballistic electrons, can be identified by applying a voltage V_{21} between leads 2 and 1, and measuring the induced voltage V_{34} between leads 3 and 4 (as shown in the left inset of Fig. 1). Electrons moving diffusively between leads 2 and 1 generate a V_{34} with the same sign of V_{21}, since the device behaves like a voltage divider, while electrons moving ballistically are injected to the opposite lead without any scattering, thus generating V_{34} with the opposite sign with respect to V_{21}.[16]

At 0 T and 4.2 K (Fig. 1), the signature of the ballistic transport was observed from the opposite sign of V_{34} with respect to V_{wire} around zero bias (region I), with a pronounced negative slope corresponding to a negative bend resistance $R_b = V_{34}/Jw_{eff}$, where J is the current density (shown in Fig. 1) and w_{eff} is the effective width of the nanowires.[16] We observed a change in the transport behavior from ballistic for $V_{wire} \ll V_{knee} \approx E_{OP}/q$ (region I) to diffusive for $V_{wire} \gg V_{knee}$ (region III), with a transition region for $V_{wire} \approx V_{knee}$ characterized by a strong non-linear behavior (region II). Such a clear signature of the electron interaction with optical phonons at E_{OP}/q (which is also confirmed by the saturation of J) along with the amplitude of the negative bend resistance offers a tool to intrinsically investigate transport and scattering mechanisms in semiconductors and heterostructures. One advantage of GaN is its much larger optical phonon energy $E_{OP} \sim 92$ meV compared to other semiconductors, allowing the investigation of transport at large bias and temperatures, in contrast to most narrow-gap semiconductors whose E_{OP} close to 25 meV leads to a strong scattering of electrons by phonons at RT.

Motivated by the similarity with the electron transport in vacuum tubes, we investigated the response of ballistic electrons in the presence of a strong magnetic field (B) perpendicular to the conductive plane between −9.9 T and 9.9 T. Fig. 2(a) shows the 2D map of V_{34} as a function of bias and magnetic field at 4.2 K. Under a perpendicular magnetic field B, the ballistic transport was modified by inducing a circular motion to electrons resulting in three distinct regions in the 2D map. (i) Ballistic region for B below 2 T: V_{34} still exhibited a negative slope but with a reduction in amplitude as B increased; (ii) high magnetic region for B above 3.6 T: the cyclotron radius was small enough to prevent the straight ballistic trajectory of electrons towards lead 3, resulting in V_{34} with the same sign of V_{21} (positive slope); and (iii) intermediate magnetic field region for B between 2 T and 3.6 T: an interesting behavior occurred for $0 < V_{wire} < V_{knee}$, where the slope of V_{34} changed from positive to negative defining sharp transition points V_{tp}, as shown in Fig. 2(b).

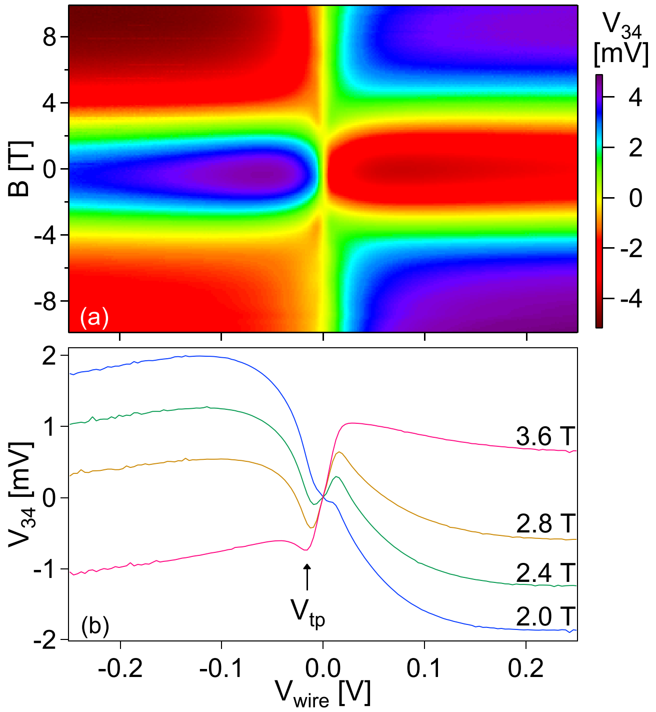

FIG. 2. (a) 2D map of V_{34} versus V_{wire} and magnetic field at 4.2 K, where it is possible to identify the three regions. (i) Ballistic region for $B < 2$ T: the influence of B is negligible and most electrons move ballistically, which is shown by the opposite sign of V_{34} with respect to V_{21}; (ii) High magnetic region for $B > 3.6$ T: electrons cannot reach the opposite lead since the magnetic curvature is the dominant effect; (iii) Intermediate magnetic region for 2 T $< B <$ 3.6 T: electrons still move ballistically but their trajectory is significantly modified by the magnetic field at low bias, which yields a circular motion. Electrons need to gain enough speed ($V_{wire} > V_{tp}$) to reach the opposite lead. (b) Plot of V_{34} versus V_{wire} for different values of magnetic field at 4.2 K where the transition points V_{tp} are indicated by the arrow.

In the absence of collisions and under a potential difference (V_{wire}), electrons move with a velocity $v = -qEt/m^*$ (where E is the electric field proportional to V_{wire} and t is the time);[18] while in the presence of a magnetic field, electrons follow a circular orbit with radius $l_c = m^* v/qB$. For $B > 2$ T and small bias, the small v of electrons yielded small l_c ($l_c \ll w$), forcing electrons in a circular ballistic motion, and resulting in a positive slope of V_{34}. As V_{wire} increased above V_{tp} for a given B, l_c became large enough to allow electrons to travel across the center of the cross and reach the opposite lead 3 ($l_c \gg w$), leading to a negative slope of V_{34}. This effect faded either with the saturation of v when $V_{wire} > V_{knee}$ or with $B > 3.6$ T, when the electron velocity is not high enough to ensure a large l_c. Hence, the turning points reflected the equilibrium between the straight motion towards lead 3 and circular motion towards lead 2 of electrons.

The absence of scattering is a required condition for the manifestation of semi-classical and quantum phenomena, which were investigated by low bias Hall measurements ($V_{\rm bias} \ll E_{\rm f}/q$) performed in the same device. Two synchronized single-output lock-in amplifiers were used for the Hall measurements: the first applied a bias of 100 μV between leads 1 and 3 and measured the current I_{13}, the second measured the Hall voltage between leads 2 and 4 (V_{24}). Fig. 3(a) shows the measured Hall resistance $R_{\rm H} = V_{24}/I_{13}$ in the device, where we observed its quenching for $|B| \lesssim 2.25$ T until relatively high temperatures (55 K). This is a direct consequence of ballistic transport of electrons at the center of the nanoscale cross. Electrons moving ballistically across the device present a probability to end up in lead 3 much higher than in leads 2 and 4, even if the Lorentz force exercised by the magnetic field imposes a preferential direction.[19] In the Büttiker and Landauer formalism $R_{\rm H} = \frac{h}{q^2}\frac{(T_2-T_4)}{[2T_3(T_3+T_2+T_4)+T_2^2+T_4^2]}$, where T_i is the transmission probability to the i-th lead.[20] The ballistic injection of electrons results in $T_3 \gg T_2 \simeq T_4 = 0$, hence $R_{\rm H} = 0\ \Omega$. In these conditions, electrons move along the transverse states,[19] where the Lorentz force does not induce a significant change in transmission probability with respect to $B = 0$ T (inset of Fig. 3(a)).

Beyond B ∼±2.25 T, the force exercised by the magnetic field is strong enough to inject electrons to a transverse lead (2 or 4 depending on the sign of B), which breaks the symmetry, raising $R_{\rm H}$ towards a second plateau. This so-called last plateau is a consequence of the absence of back-scattering due to guiding of electrons through edge states when $l_c \leq w_{\rm eff}$. This occurs for $B < B_0 = \hbar k_{\rm F}/e w_{\rm eff}$ ($w_{\rm eff}$ is the effective width of the channel), when the Hall resistance saturates at $R_{\rm H_0} = \frac{h}{2q^2}\frac{\pi}{k_{\rm F} w_{\rm eff}}$, which is the quantum resistance of a quasi-1D nanowire.[21] The independence of the $R_{\rm H}$ on B holds until $2l_c < w$, thus for $B_0 < B < 2B_0$.

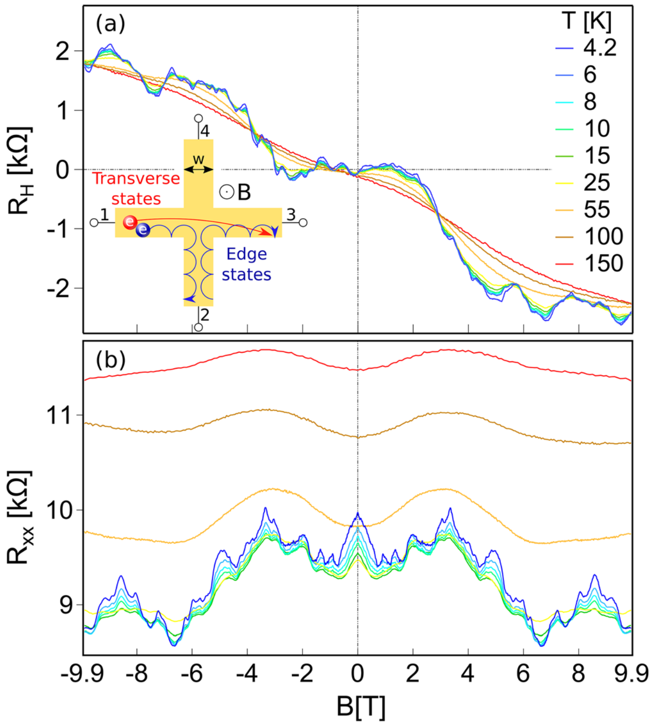

FIG. 3. (a) $R_{\rm H}$ versus magnetic field at different temperatures. The inset shows the schematic of device for the Hall measurement along with a geometric interpretation of the difference between transverse and edge states. (b) $R_{\rm xx}$ versus magnetic field at different temperatures.

To evaluate B_0 and $R_{\rm H_0}$, $w_{\rm eff}$ was determined from the plot of the longitudinal resistance $R_{\rm xx} = V_{13}/I_{13}$ versus B (Fig. 3(b)). The shoulders observed in $R_{\rm xx}$ at $B_s = \pm 3.34$ T were a consequence of back-scattering of electrons, a geometrical phenomenon responsible for the observed peaks in $R_{\rm xx}$ when $w_{\rm eff} \sim 0.55 l_c$.[22,23] This relationship resulted in $w_{\rm eff} = \hbar k_{\rm F}/qB_s = 48$ nm, $B_0 = 6.1$ T, and $R_{\rm H_0} = 1.92$ kΩ, in excellent agreement with our experimental results (Fig. 3(a)). We could not observe the end of the last plateau, since $2B_0 = 12.2$ T was not achievable with our experimental set-up.

From $w_{\rm eff}$, we estimated a small sidewall depletion of 19.5 nm in AlGaN/GaN, which highlights another advantage of this material for the study of ballistic transport in top-down etched nanoscale devices. The fluctuations observed in $R_{\rm xx}$ and in $R_{\rm H}$ as well as the peak observed in $R_{\rm xx}$ at 0 T were signatures of universal conductance fluctuations (UCF)[24,25] and weak localization (WL),[15,26] respectively. The variance of UCF was used to extract a phase coherence length (l_φ) of 190 nm.[24,25] The much larger l_φ compared to w supports the quantum interference observed up to ∼25 K which resulted in WL and UCF (Figs. 3(a) and 3(b)). At larger temperatures, the thermal energy smeared out all these magneto-anomalies resulting in classic-like Hall behavior. Hall measurements also allowed us to determine the carrier density in the 2DEG in the nanoscale cross. In classical Hall effect, the Hall resistance depends on B as $R_{\rm H} = B/(qn_s)$ yielding $n_s = 3.1 \times 10^{12}\,{\rm cm}^{-2}$ at 4 K (in this case a larger bias of 300 mV was used to avoid the presence of quantum fluctuations) and $2.78 \times 10^{12}\,{\rm cm}^{-2}$ at 300 K. The smaller values of n_s in the nanoscale cross compared to bulk values were due to sidewall depletion and strain relaxation of the AlGaN barrier in narrow structures.[27] The estimated l_m using these values of n_s was 51 nm at 300 K and 313 nm at 4 K.

In conclusion, nanoscale ballistic filters, fabricated using state-of-the-art top-down nanofabrication technology, were used to investigate the electron transport, as well as semi-classical and quantum effects in AlGaN/GaN heterostructures. Electron transport was investigated under a transverse magnetic field to manipulate the trajectory of electrons under ballistic regime. In high-bias condition, a strong dependence of V_{34} on both magnetic field and bias voltage resulted in transition points (for 2 T $< B <$ 3.6 T) with a pronounced non-linear behavior revealing the equilibrium between straight and circular trajectories of ballistic electrons.

We also correlated the ballistic behavior with semi-classical and quantum effects by measuring the same device in a Hall configuration, which highlighted the interaction of the scattering-less ballistic transport with Lorentz forces in bending the electron trajectory and creating edge states for electron propagation. Hall measurements revealed the quenching of Hall resistance and the manifestation of the last plateau (saturation of the Hall resistance) in excellent agreement with the theoretical value of the quasi-1D resistance $R_{\rm H_0}$. A large measured phase coherence length of

190 nm allowed the observation of universal quantum fluctuations and weak localization due to quantum interference up to ~25 K.

This work shows the manifestation of classical, semi-classical, and quantum phenomena due to the interaction between electrons moving under ballistic regime and a strong magnetic field perpendicular to the conduction plane. In addition, it reveals the prospect of the wide band-gap GaN semiconductors as a platform for basic transport and quantum studies under large bias and high temperature, as well as of nanoscale ballistic crosses as a tool to intrinsically investigate transport and scattering mechanisms in semiconductors and heterostructures.

We thank the precious support from Professor Andras Kis from EPFL for the use of his cryogenic setup and the insightful discussions. G.S. and E.M. thank Professor Klaus Enslim from ETH for valuable insights and Pulkit Tandon for initial discussions leading to the experiment. The authors declare no competing financial interests.

[1] O. Celik, E. Tiras, S. Ardali, S. Lisesivdin, and E. Ozbay, Open Phys. **10**, 485–491 (2012).
[2] A. M. Song, P. Omling, L. Samuelson, W. Seifert, I. Shorubalko, and H. Zirath, Jpn. J. Appl. Phys., Part 2 **40**, L909 (2001).
[3] Q. Diduck, H. Irie, and M. Margala, Int. J. High Speed Electron. Syst. **19**, 23 (2009).
[4] M. Seo, C. Hong, S.-Y. Lee, H. K. Choi, N. Kim, Y. Chung, V. Umansky, and D. Mahalu, Sci. Rep. **4**, 3806 (2014).
[5] J. Herfort, Y. Takagaki, R. Hey, K.-J. Friedland, K. Ploog, D. K. Maude, J. C. Portal, J. Takahara, and K. Gamo, J. Phys.: Condens. Matter **7**, 9563 (1995).
[6] A. M. Gilbertson, A. Kormányos, P. D. Buckle, M. Fearn, T. Ashley, C. J. Lambert, S. A. Solin, and L. F. Cohen, Appl. Phys. Lett. **99**, 242101 (2011).
[7] S. Chuang, Q. Gao, R. Kapadia, A. C. Ford, J. Guo, and A. Javey, Nano Lett. **13**, 555 (2013).
[8] U. Wieser, S. A. Poenariu, U. Kunze, and T. Hackbarth, Appl. Phys. Lett. **87**, 252114 (2005).
[9] B. J. Van Wees, H. Van Houten, C. W. J. Beenakker, J. G. Williamson, L. P. Kouwenhoven, D. Van der Marel, and C. T. Foxon, Phys. Rev. Lett. **60**, 848 (1988).
[10] R. de Picciotto, H. L. Stormer, L. N. Pfeiffer, K. W. Baldwin, and K. W. West, Nature **411**, 51 (2001).
[11] H. Van Houten, C. W. J. Beenakker, J. G. Williamson, M. E. I. Broekaart, P. H. M. Van Loosdrecht, B. J. Van Wees, J. E. Mooij, C. T. Foxon, and J. J. Harris, Phys. Rev. B **39**, 8556 (1989).
[12] G. Timp, H. U. Baranger, J. E. Cunningham, R. E. Howard, R. Behringer, P. M. Mankiewich *et al.*, Phys. Rev. Lett. **60**, 2081 (1988).
[13] S. Sasaki, Y. Hirayama, and S. Tarucha, Jpn. J. Appl. Phys., Part 1 **34**, 1351 (1995).
[14] C. J. B. Ford, T. J. Thornton, R. Newbury, M. Pepper, H. Ahmed, D. C. Peacock, D. A. Ritchie, J. E. F. Frost, and G. A. C. Jones, Phys. Rev. B **38**, 8518 (1988).
[15] T. J. Thornton, M. Pepper, H. Ahmed, D. Andrews, and G. J. Davies, Phys. Rev. Lett. **56**, 1198 (1986).
[16] E. Matioli and T. Palacios, Nano Lett. **15**, 1070 (2015).
[17] U. Rössler, in *Quantum Transport in Ultrasmall Devices*, NATO ASI Series No. 342, edited by D. K. Ferry, H. L. Grubin, C. Jacoboni, and A.-P. Jauho (Springer US, 1995), pp. 77–109.
[18] S. L. Teitel and J. W. Wilkins, IEEE Trans. Electron Devices **30**, 150 (1983).
[19] A. M. Chang, T. Y. Chang, and H. U. Baranger, Phys. Rev. Lett. **63**, 996 (1989).
[20] H. U. Baranger and A. D. Stone, Phys. Rev. Lett. **63**, 414 (1989).
[21] *Electronic Properties of Multilayers and Low-Dimensional Semiconductor Structures*, NATO ASI Series, edited by J. M. Chamberlain, L. Eaves, and J.-C. Portal (Springer US, Boston, MA, 1990), Vol. 231.
[22] T. J. Thornton, M. L. Roukes, A. Scherer, and B. P. Van de Gaag, Phys. Rev. Lett. **63**, 2128 (1989).
[23] C. W. J. Beenakker and H. van Houten, Solid State Phys. **44**, 1 (1991).
[24] C. W. J. Beenakker and H. van Houten, Phys. Rev. B **37**, 6544 (1988).
[25] P. A. Lee, A. D. Stone, and H. Fukuyama, Phys. Rev. B **35**, 1039 (1987).
[26] J. A. Katine, M. J. Berry, R. M. Westervelt, and A. C. Gossard, Phys. Rev. B **57**, 1698 (1998).
[27] M. Azize and T. Palacios, Appl. Phys. Lett. **98**, 042103 (2011).